Article

Paramagnetic Lipid-Coated Silica Nanoparticles with a Fluorescent Quantum Dot Core: A New Contrast Agent Platform for Multimodality Imaging

Rolf Koole, Matti M. van Schooneveld, Jan Hilhorst, Karolien Castermans, David P. Cormode, Gustav J. Strijkers, Celso de Mello Donega#, Daniel Vanmaekelbergh, Arjan W. Griffioen, Klaas Nicolay, Zahi A. Fayad, Andries Meijerink, and Willem J. M. Mulder

Bioconjugate Chem., **2008**, 19 (12), 2471-2479 • DOI: 10.1021/bc800368x • Publication Date (Web): 26 November 2008

Paramagnetic Lipid-Coated Silica Nanoparticles with a Fluorescent Quantum Dot Core: A New Contrast Agent Platform for Multimodality Imaging

Rolf Koole,[†] Matti M. van Schooneveld,[†] Jan Hilhorst,[†] Karolien Castermans,[‡] David P. Cormode,[§] Gustav J. Strijkers,[||] Celso de Mello Donegá,[†] Daniel Vanmaekelbergh,[†] Arjan W. Griffioen,[‡] Klaas Nicolay,[||] Zahi A. Fayad,[§] Andries Meijerink,[†] and Willem J. M. Mulder*[,§]

Condensed Matter and Interfaces, University Utrecht, P.O. Box 80000, 3508 TA Utrecht, The Netherlands, Angiogenesis Laboratory, Research Institute for Growth and Development, Department of Pathology/Internal Medicine, Maastricht University and University Hospital, P.O. Box 5800, 6202 AZ Maastricht, The Netherlands, Translational and Molecular Imaging Institute and Imaging Science Laboratories, Mount Sinai School of Medicine, One Gustave L. Levy Place, New York, New York 10029, and Biomedical NMR, Department of Biomedical Engineering, Eindhoven University of Technology, P.O. Box 513, 5600 MB Eindhoven, The Netherlands.
Received August 28, 2008; Revised Manuscript Received October 27, 2008

Silica particles as a nanoparticulate carrier material for contrast agents have received considerable attention the past few years, since the material holds great promise for biomedical applications. A key feature for successful application of this material in vivo is biocompatibility, which may be significantly improved by appropriate surface modification. In this study, we report a novel strategy to coat silica particles with a dense monolayer of paramagnetic and PEGylated lipids. The silica nanoparticles carry a quantum dot in their center and are made target-specific by the conjugation of multiple $\alpha v\beta 3$-integrin-specific RGD-peptides. We demonstrate their specific uptake by endothelial cells in vitro using fluorescence microscopy, quantitative fluorescence imaging, and magnetic resonance imaging. The lipid-coated silica particles introduced here represent a new platform for nanoparticulate multimodality contrast agents.

INTRODUCTION

Nanoparticles have been explored for a few decades now as vehicles to deliver therapeutic agents (*1*). Traditionally, nanoparticles composed of naturally occurring molecules, such as bilayered vesicles composed of phospholipids, have been utilized (*2*). The revolution in nanoscience has resulted in the development of a tremendous amount of new materials that hold great potential for biomedical applications (*3*). In the field of diagnostic imaging, nanoparticles also create new possibilities. These include iron oxide nanoparticles for magnetic resonance imaging (MRI) (*4*), carbon nanotubes for MRI (*5*), or gold nanoparticles for computed tomography (CT) (*6*). Semiconductor nanocrystals, also known as quantum dots (QDs), have been recognized as an optical contrast agent due to their outstanding fluorescent properties (*7*). A major advantage of the application of nanoparticles for biomedical purposes is that they can have multiple properties integrated within one single carrier particle. In addition, the possibilities for surface modification create flexibility for a large range of applications. The above-mentioned features of nanoparticles have resulted in the development of nanoparticles that are suitable for both therapeutic and diagnostic purposes (*8*), as well as nanoparticles that can be employed for different imaging modalities, so-called multimodality nanoparticles (*9*).

Silica as a nanoparticulate carrier material has received considerable attention the past few years. The incorporation of nanoparticles in silica has been reported for semiconductor (*10, 11*), metallic (*12, 13*), and magnetic nanocrystals (*14*). In addition, the simultaneous incorporation of magnetic nanoparticles and QDs in silica nanospheres has been reported recently (*15*−*18*). Doping of silica particles with dye molecules is well-established (*19*−*21*), while combinations of dyes with other functionalities within one silica sphere have also been reported (*22*−*24*). The use of these silica-coated nanoparticles and/or dyes as contrast agents for bioimaging applications benefits from the high versatility and well-known surface chemistry of silica nanospheres (*25*). The possibility of combining multiple properties within one silica nanosphere as well as the control over the final particle size over a broad range (20 nm to 5 μm) make these composite particles especially suitable as carriers for multiple diagnostically active materials (*26*−*29*). Most importantly, a key feature for successful application of this material in vivo is biocompatibility, which may be significantly improved by appropriate surface modification.

Two distinct surface modifications to enhance the bioapplicability of silica nanospheres have been reported to date, which both depend on the use of silane coupling agents. In the first method, the silica spheres are terminated by an amine or thiol group using APS or MPS (aminopropyltrimethoxysilane and mercaptopropylmethoxysilane), to which biofunctional groups can be covalently linked (*24, 30*−*34*). The second method involves the modification of the silica surface by molecules that already have a silane group integrated within the molecule (*24, 32, 34, 35*). Most of the aforementioned reports use both strategies simultaneously to attach functional moieties, including antibodies, paramagnetic molecules, and poly(ethylene glycol) (PEG), through an amide bond. Although some variation in surface functionalization is possible, there are several serious drawbacks for these methods. First, due to steric hindrance and differences in reactivity with coupling agents, it is not clear to what extent

* Corresponding author. Willem Mulder, e-mail: willem.mulder@mountsinai.org; tel: 2122417717; fax: +1 212 534 2683.
[†] University Utrecht.
[‡] Maastricht University and University Hospital.
[§] Mount Sinai School of Medicine.
[||] Eindhoven University of Technology.

10.1021/bc800368x CCC: $40.75
Published on Web 11/26/2008

and in what ratio the silica surface is covered by the pegylated and biofunctional molecules. Second, the density of the (pegylated) coating around the silica spheres is not well-defined, which limits the optimal use of the surface area payload and may lead to suboptimal biocompatibility. In addition, depending on the pH, this methodology results in the presence of negatively positively charged hydroxyl/amine groups, which may unfavorably affect the stability under physiological conditions. Third, the flexibility of these methods is limited to molecules with reactive groups for the covalent linking step.

In the current study, we report a novel strategy to coat silica particles with a dense monolayer of lipids without the usage of (silane) coupling agents. In the first step, the silica particles are rendered hydrophobic, after which they are coated with both paramagnetic and PEGylated lipids in a second step. This highly flexible and widely applicable coating method for silica particles also allows for the conjugation of target-specific molecules at the surface of the nanoparticle. In the present case, we use highly monodisperse silica particles that have a single core−shell−shell (CSS) QD incorporated into the center and paramagnetic Gd-DTPA-DSA in the lipid coating, to enable their detection with both fluorescence techniques and MRI. As a proof-of-principle, we demonstrate target-specific multimodality imaging of $\alpha v\beta 3$-integrin expression on cultured endothelial cells using our lipid-coated QD/silica nanoparticles.

EXPERIMENTAL PROCEDURES

Materials. 1,2-Distearoyl-*sn*-glycero-3-phosphoethanolamine-*N*-[methoxy(poly(ethylene glycol))-2000] (PEG-DSPE) and 1,2-distearoyl-*sn*-glycero-3-phosphoethanolamine-*N*-[maleimide-(poly(ethylene glycol))2000] (Mal-PEG-DSPE) were purchased from Avanti Polar Lipids. Gd-DTPA-bis(stearylamide) (Gd-DTPA-DSA) was obtained from Gateway Chemical Technology. Methanol (anhydrous, 99.8%), octadecanol (99%), Igepal (CO-520), oleic acid (90%), octadecylamine (ODA 97%), and octadecene (ODE, 90%) were purchased from Aldrich. Tetraethyl orthosilicate (TEOS, 99%) was obtained from Johnson Matthey. Acetone (p.a.), chloroform (p.a.), ammonia (25% in water, p.a.), cadmium oxide (>99%), zinc oxide (>99%), and HEPES ($C_8H_{18}N_2O_4S$, >99%) were purchased from Merck. The HEPES buffer contained 2.38 g/L HEPES and 8.0 g/L NaCl (99.8%, Baker), and the pH was adjusted to 6.7 by addition of a NaOH solution. Sulfur powder (99.999%) was obtained from Alfa Aesar, and ethanol (>99.8%) from Riedel de Haën. The cyclic 5-mer RGD (c(RGDf(-S-acetylthioacetyl)K)) was synthesized at a purity of 95% by Ansynth Service BV (The Netherlands).

Synthesis of Silica-Coated QDs. CdSe (core) QDs (3.4 nm in diameter) were synthesized by the conventional organometallic synthesis route, described in detail elsewhere (*36*). The CdSe QDs were coated with 7 monolayers of inorganic shells ($2 \times$ CdS, $3 \times Cd_{0.5}Zn_{0.5}S$, $2 \times$ ZnS) according to a SILAR method that was recently published by Xie et al. (*37*). Addition of these shells was performed by adding precalculated amounts of a 0.1 M precursor solution (Cd oleate, CdZn oleate, Zn oleate, and sulfur in ODE) to 200 nmol CdSe QDs dispersed in a mixture of 4.5 mL ODE and 1.5 mL ODA at 230 °C. Each monolayer was allowed to grow for 10 min before the next precursor solution was added). The CSS-QDs were purified by precipitation and redispersion in a chloroform/acetone mixture 3 times. The resulting core−shell−shell (CSS) QDs increased in size to 7.7 nm (±0.9 nm) and were photostable in air for months, with a QY of 60%. The CSS-QDs were incorporated in silica spheres by a reverse microemulsion method (*10*). In short, 1.3 mL Igepal was added to 10 mL cyclohexane and stirred for 15 min (850 rpm). Subsequently, 2 nmol of QDs (in 100 μL cyclohexane), 80 μL TEOS, and 150 μL ammonia was added with 15 min of stirring in between the additions. After the last addition, the mixture was stirred for 1 min, after which it was placed in the dark for 1 week. The resulting silica-coated QDs were centrifuged and redispersed in ethanol at least 3 times to remove excess reactants from the silica synthesis (i.e., Igepal, TEOS, ammonia, and water).

Lipid Coating of Silica Particles. The silica-coated QDs were subsequently capped with a hydrophobic ligand, by adding an excess of octadecanol (ODOH, 2.5 g in 5 mL of EtOH) to a dispersion of 2 nmol of silica-coated QDs in 5 mL ethanol. This mixture was first heated to 100 °C for 1 h to remove the ethanol, after which the temperature was raised to 170 °C for 3 h to covalently link the ODOH to the silica spheres by a condensation reaction (*38*). The QY of the CSS QDs and ODOH coated QD/silica particles was determined by integrating the emission spectra of these samples (in chloroform) and comparing it to the integrated emission of both Rhodamine 6G and Rhodamine 101 (assuming a QY of 90% and 95% for these dyes, respectively). Each emission spectrum was corrected for the relative absorbance of the sample at the excitation wavelength (497 nm in case of Rhodamine 6G and 528 nm in case of Rhodamine 101). Next, the ODOH-coated silica nanoparticles (with a QD incorporated) were dispersed in chloroform/methanol (20/1, v/v). PEG-DSPE, Mal-PEG-DSPE, and Gd-DTPA-DSA were added in a molar ratio of 0.4/0.1/0.5. The amount of lipids was 25 times higher than the calculated amount of lipids for a monolayer on all nanoparticles. This solution was added to a mildly basic HEPES buffer (20 mM HEPES, 135 mM NaCl, pH 6.7) under vigorous stirring, which led to the formation of an emulsion that was subsequently heated to 110 °C to evaporate chloroform. Upon evaporation of chloroform, the milky suspension converted into a clear dispersion indicative of the total removal of chloroform and the formation of lipid-coated QD/silica nanoparticles. The excess of lipids was removed by centrifugation (3000 rpm) of the lipid-coated QD/silica particles, which were redispersed in HEPES buffer. The cyclic 5mer RGD (c(RGDf(-S-acetylthioacetyl)K)) was conjugated to Mal-PEG-DSPE included in the lipid layer as described previously (*39*). In short, acetyl-protected peptide was deacetylated in 0.05 M Hepes/0.05 M hydroxylamine-HCl/0.03 mM ethylenediamine tetraacetic acid (pH 7.0) for 1 h at room temperature. The activated peptide was added to the Mal-PEG2000-DSPE containing particles. This preparation was stored at 4 °C under N_2 overnight.

Transmission Electron Microscopy (TEM) and Dynamic Light Scattering (DLS). A Tecnai 10 (FEI Company) transmission electron microscope, operated at an acceleration voltage of 100 kV, was used to take bright-field images. Samples were prepared for negative staining by exchanging the buffer for a 0.125 M ammonium acetate and 0.26 mM EDTA adjusted to pH 7.4. This solution was then mixed in a 1:1 ratio with a 2% sodium phosphotungstate negative stain solution (pH 7.4). Formvar-coated nickel grids were dipped in this solution and imaged shortly afterward. The TEM micrographs were processed using TIA software (Tecnai imaging and analysis software). Measurement of the size distribution of the ODOH coated QD/silica particles in chloroform and the Q-SiPaLCs suspended in deionized water was performed with a Malvern HPPS DLS (dynamic light scattering) instrument equipped with a He−Ne laser operating at 633 nm.

In Vitro Targeting Experiments. Human umbilical vein derived endothelial cells (HUVEC) were cultured on gelatin (0.2% in PBS) coated tissue culture flasks (Costar, Cambridge, MA) in culture medium, RPMI-1640 (Life Technologies, Breda, The Netherlands), 10% human serum, and 10% fetal calf serum (HS and FCS; University Hospital Maastricht, The Netherlands), 2 mM glutamine (Life Technologies), 50 U/mL penicillin, and

Scheme 1. Overview of the Multistep Synthesis of Q-SiPaLCs[a]

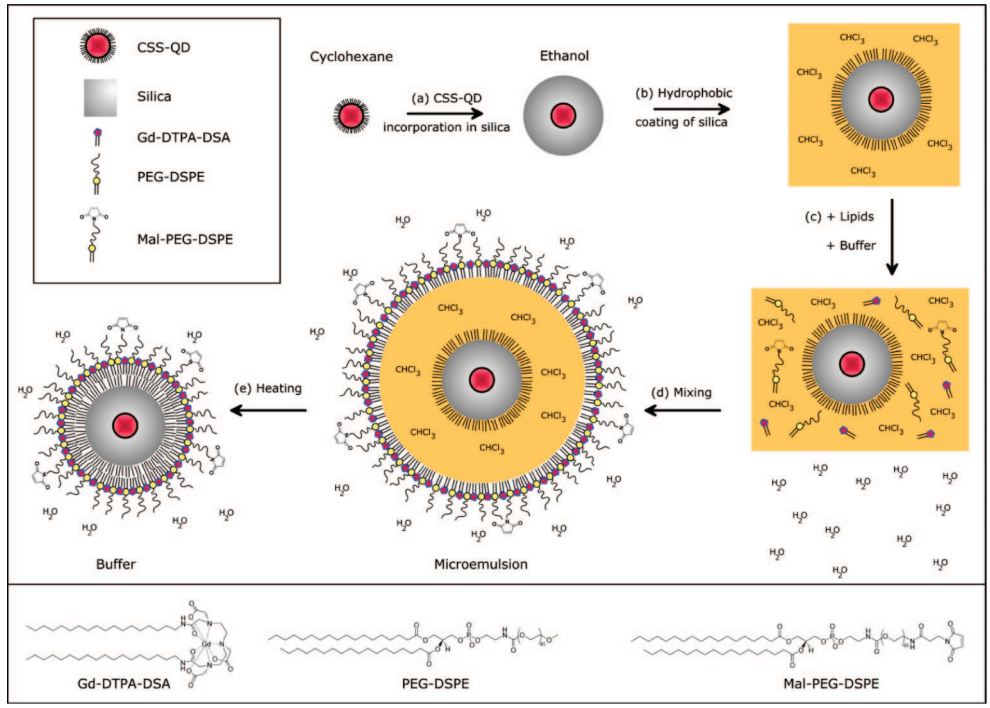

[a] (a) Incorporation of CSS-QDs in silica spheres by the reverse micelle method. (b) Hydrophobic coating of silica by ODOH, after which they can be dispersed in chloroform. (c) Addition of the different lipids to the QD/silica particles in chloroform, which is subsequently added to a HEPES buffer. (d) Vigorous stirring results in an emulsion, with the chloroform and nanoparticles enclosed in a lipid monolayer. (e) Chloroform is evaporated by heating the mixture, resulting in water-soluble Q-SiPaLCs. See Experimental Procedures section for details. The lower panel displays the structure formulas of the lipids.

50 ng/mL streptomycin (ICN Biomedicals, Aurora, OH). For all incubations, 1.5×10^6 cells of passage 2−3 were used for experiments (at least $n = 2$). The cells were incubated for 8 h with RGD conjugated nanoparticles or control nanoparticles at a concentration of 0.07 nmol particles/mL medium. Association of the different nanoparticles to endothelial cells was assessed using fluorescence microscopy and magnetic resonance imaging. A Leica DMIL phase contrast fluorescence microscope (Leica Microsystems, Rijswijk, The Netherlands) equipped with a 20 W G4 HXL64250 Xenophot Halogen lamp (Leica) was used. Parallel phase contrast and red fluorescence (using a BP645−675 filter, Leica) images of the endothelial cell monolayers were taken at 200× magnification. All fluorescence microscopy scans were made with the same settings for laser power and detector sensitivity, allowing direct comparison between different incubations. The cell density for both incubations in Figure 2 was comparable, and therefore, the difference in fluorescence intensity arises from the difference in the level of association.

Fluorescence Imaging and MRI. Fluorescence imaging of cell pellets was performed using the Xenogen IVIS-200 small animal imaging system. A continuous external light source of 365 nm and an emission filter 610−630 nm were used.

MRI experiments were performed on a 6.3 T horizontal bore magnet (Oxford Instruments, England) interfaced to a Bruker (Bruker, Ettlingen, Germany) MR imaging console. A 3 cm quadrature-driven birdcage coil was used. The cups containing cell pellets were placed in a custom-made sample holder, capable of carrying 4 Eppendorf cups. For absolute quantification of T1, an inversion recovery fast T1-mapping sequence was used with 80 different inversion times. In the experiment, TR was 20 s, TE was 9 ms, and the slice thickness was 0.7 mm. For absolute quantification of T2, a multi-spin−echo sequence was used with TR 2000 ms and 32 echos that had a 9 ms echo spacing. A T1-weighted image of cell pellets of the three incubations was generated with a TR of 1500 ms. In this image, cells with a high content of Gd appear brighter than cells with a low content of Gd or no Gd. In all the MRI experiments, the FOV was 3 cm^2, the matrix size 128 × 128 voxels, and the slice thickness 0.7 mm.

RESULTS

Highly photostable and luminescent CdSe/CdS/$Cd_{0.5}Zn_{0.5}S$/ZnS core−shell−shell (CSS) QDs were synthesized according to a SILAR procedure reported by Xie et al. (*37*) Subsequently, a reverse micelle method reported earlier (*10, 11*) was used to incorporate QDs in the center of highly monodisperse silica particles of 31 nm (±4 nm); see Figure 1A. The synthesis involved the dispersion of hydrophobic QDs in cyclohexane, to which a nonionic surfactant (Igepal), a silane precursor (TEOS, tetraethyl orthosilacate), and catalyst (ammonia) were added. The exact incorporation mechanism and details on the synthesis are published elsewhere (*40*). In short, hydrolyzed TEOS present in the initial reaction mixture (before adding ammonia) replaces the hydrophobic ligands on the QDs. The TEOS-coated QDs are then transferred to the hydrophilic interior of the reverse micelles, where subsequent silica growth takes place. The majority of the silica particles contained a single QD in the center, while only a small fraction of the silica particles contained 2 or more QDs per particle (Figure 1A). Although the QD/silica particles thus obtained are soluble in ethanol or water, the pharmacokinetics of charged surface particles are unfavorable, typically due to a short circulation half-life and/or accumulation in the lungs (*41, 42*). In order to obtain bioapplicability by a dense lipid coating, the QD/silica particles were first made hydrophobic by an octadecanol (ODOH) coating. This was achieved using a well-known condensation reaction (*38*), where the alcohol group of ODOH reacts with the hydroxyl groups at the silica surface to form a covalent bond, neutralizing the surface charges. The hydrophobic QD/silica particles were subsequently coated with a dense

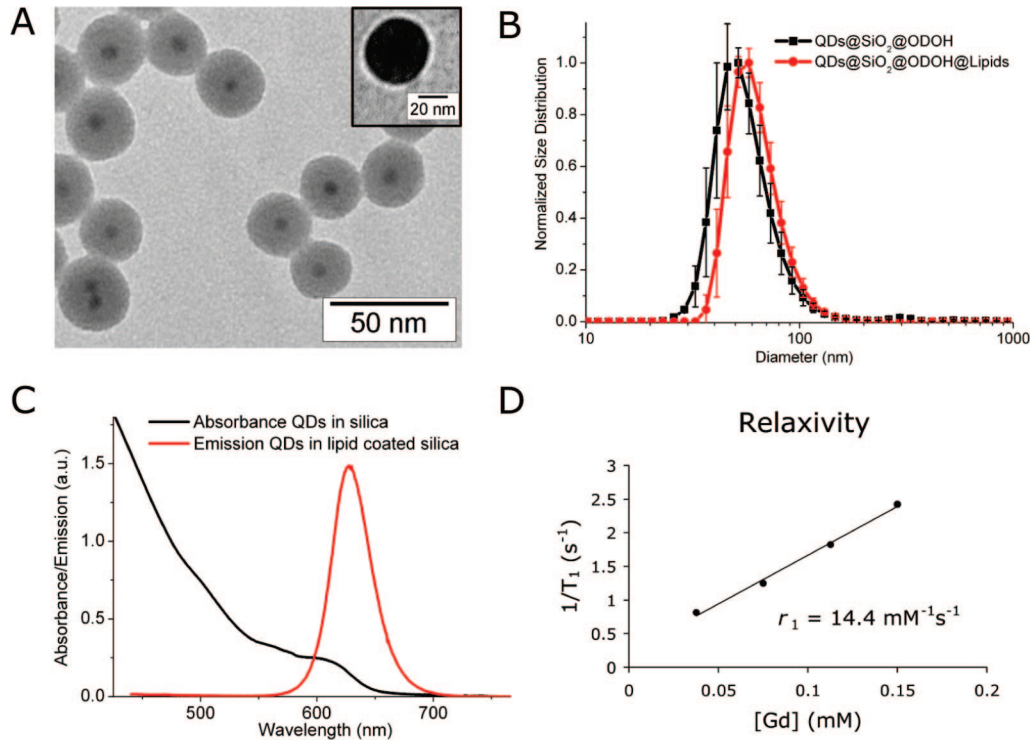

Figure 1. (A) TEM image of monodisperse QD/silica particles of 31 nm (±4 nm) with a single QD (7.7 nm, black spots) incorporated in the center. Inset shows an image from negative staining TEM, where the bright corona illustrates the hydrophobic layer around the silica particle. (B) DLS of ODOH capped QD/silica nanoparticles and ODOH capped QD/silica nanoparticles encapsulated in lipids. (C) Absorption and emission spectra of the CSS-QDs in silica. (D) Relaxation rates of the Q-SiPaLCs as a function of the concentration of Gd^{3+} ions (determined by ICP-MS).

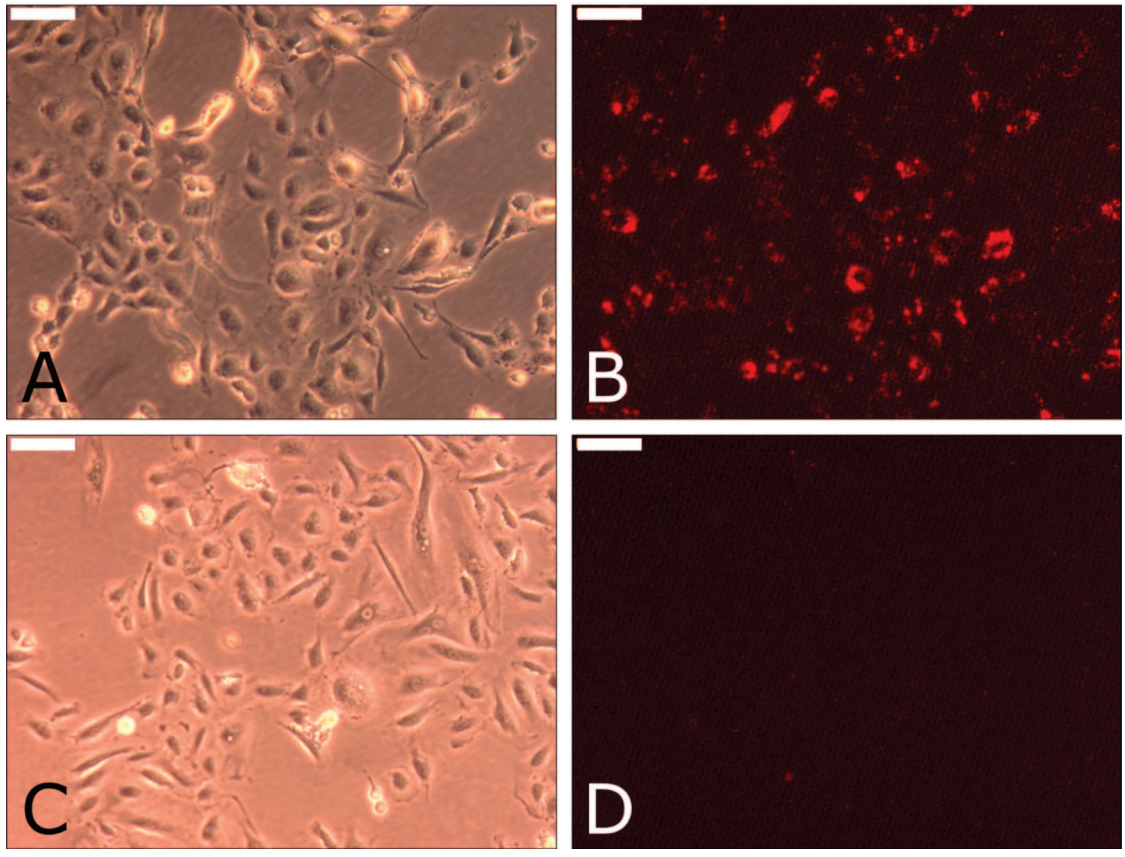

Figure 2. (A,C) Bright-field microscopy images and (B,D) fluorescence microscopy images of HUVEC incubated with (A,B) RGD-conjugated nanoparticles or (C,D) non-conjugated (untargeted) nanoparticles. The scale bars correspond to 100 μm.

monolayer of lipids using a simple and fast procedure reported earlier for hydrophobic nanocrystals (*39, 43*). The procedure involves the addition of lipids and water to the hydrophobic QD/silica particles in chloroform, followed by the evaporation

of chloroform, leaving behind a clear suspension of well-dispersed, uncharged silica particles in lipidic micelles. The total synthesis procedure is schematically summarized in Scheme 1. The lipid coating is versatile, because in principle any (functional) amphiphile may be incorporated in this lipid layer. As an example, we have used a combination of Gd-DTPA-based lipids to introduce paramagnetic properties for MRI, pegylated lipids to improve biocompatibility, and maleimide-terminated (pegylated) lipids for conjugation of a biofunctional group. We will refer to the synthesized QDs in silica with a paramagnetic lipidic coating as Q-SiPaLCs.

The nanoparticles were characterized in terms of their size and optical and magnetic properties. We performed transmission electron microscopy (TEM) and negative staining TEM (Figure 1A) as well as dynamic light scattering (DLS) measurements to determine the morphology and size of the silica particles before and after applying the lipid coating. Negative stain TEM (which allows the visualization of hydrophobic substances) images were analyzed, revealing a hydrophobic layer of 3.9 nm ($\pm$0.5 nm) around individual particles, illustrated by the bright corona around the silica particle (Figure 1A, inset). This 4-nm-thick hydrophobic layer confirms the presence of both the ODOH coating around silica ($\sim$2 nm) and the stearyl chains of the lipids ($\sim$2 nm) around the particles. As well as size determinations established by TEM, the size of nanoparticles in an aqueous environment can be estimated using dynamic light scattering (DLS). This so-called hydrodynamic diameter was determined to be 50 nm for ODOH coated QD/silica particles, increasing to 58 nm after the application of the lipid coating (Figure 1B). This increase is in reasonable agreement with what one may expect in the case a single silica nanoparticle is coated with both paramagnetic lipids ($\sim$2 nm) and pegylated lipids ($\sim$10 nm). Figure 1C displays the absorption and emission spectra. The emission spectrum is shown for the final Q-SiPaLCs in HEPES buffer. The absorption spectrum in Figure 1C was measured for the QDs in silica with an octadecanol coating, dispersed in chloroform. The latter system is refractive-index matched (in contrast to the Q-SiPaLCs in water), allowing for a scattering-free absorption measurement and reliable determination of the quantum yield (QY). The absorption spectrum displays multiple absorption features as a result of discrete excitonic transitions in the CSS-QDs, which can be observed due to the high quality and monodispersity of the QDs. The initial QY of the CSS-QDs was 60%, but decreased as a result of the silica coating. This decrease is difficult to measure due to the scattering of the silica particles in ethanol, but it is estimated that the QY after silica coating is 25%. Coating the QD/silica particles with ODOH increased the QY to 35%, which could be accurately determined because of the scattering-free dispersion of the hydrophobic particles in chloroform. The QY of the lipid-coated QD/silica particles in water was slightly lower (by eye), which was again difficult to quantify due to scattering. It should be noted that a significant QY enhancement of the silica-coated QDs is observed upon UV illumination (which was avoided here when determining the QY, to obtain the lower limit). The silica coating and further coating steps did not change the shape of absorption or emission spectra of the QDs. A detailed discussion on the evolution of the QY of the QDs upon incorporation in silica and photoactivation is published elsewhere (*40*). The emission maximum of the CSS QDs lies at 630 nm. This relatively long wavelength is favorable for in vivo fluorescence imaging because of the lower autofluorescence levels of tissue for longer-wavelength excitation and the longer penetration depth into tissue of light with this wavelength.

To make the particle also suitable as an MRI contrast agent, Gd-DTPA-DSA was included in the lipidic coating of the Q-SiPaLCs. This paramagnetic amphiphile consists of Gd-DTPA, a clinically used contrast agent for MRI, and two saturated acyl chains with a chain length of 18 carbon atoms. To evaluate the performance as an MRI contrast agent, the longitudinal relaxation rates R1 of a dilution series were determined at 60 MHz, and Gd contents of these samples were determined by ICP-MS. From these data, the longitudinal relaxivity r1 of the Gd^{3+} ions was calculated to be 14.4 mM^{-1} s^{-1} (Figure 1D), which is a factor of 3$-$4 higher than free Gd-DTPA molecules in solution. This difference is ascribed to the lower tumbling rate of the Gd-lipids in the micelle compared to free Gd-DTPA molecules, enhancing the molar relaxivity (*35, 39, 44*).

As mentioned above, the number of Gd ions was determined by ICP-MS for a dispersion of Q-SiPaLCs. The concentration of Q-SiPaLCs in this dispersion was estimated from the initial number of QDs used for the silica synthesis at 0.24 μM. We found with ICP-MS that the concentration of Gd in the same dispersion was 0.60 mM, which gives a number of 2500 Gd-lipids per silica particle. The estimated maximum number of lipids in a densely packed lipid layer surrounding a 31 nm silica particle is approximately 5000, using a literature value of 60 A^2/lipid (*45*). Since half of the lipids consisted of Gd-DTPA-DSA, the estimated (2500) and experimentally determined (2500) number of Gd-lipids are in excellent agreement, confirming a dense coating of lipids around the Q-SiPaLCs. This is further confirmed by the number of Cd ions that was determined for the same dispersion using ICP-MS, which was found to be 0.50 mM. The number of Cd ions per CSS QD can be estimated to be approximately 2200, by assuming an average wurtzite unit cell volume of 1.1×10^{-28} m^3 (for CdSe, CdS, and CdZnS) with $Z = 2$ and taking into account the presence of Zn ions in the outer shells. Assuming a number of 2200 Cd ions per QD, the concentration of QDs in the dispersion is estimated to be 0.23 μM, which correlates well with the estimation above.

Taking into consideration that the 31 nm Q-SiPaLCs thus carry approximately 2500 Gd-DTPA-DSA lipids per particle (average between calculated and experimentally determined value), the r1 relaxivity per particle was estimated to be 36 000 mM^{-1} s^{-1}. The relaxivity of the Q-SiPaLCs per particle is thereby a factor of 21 higher than for our previously reported lipid-coated QDs (*39*), and a factor of 8$-$12 higher than Gd-wedge-coated QDs that were recently reported (*46*). In another recent report, the relaxivity of Gd-DOTA covalently attached to silica was determined to be 23 mM^{-1} s^{-1}, and apart from the lower tumbling rate, the very high relaxivity was ascribed to a higher water density close to the Gd-DOTA complexes due to the absence of lipids (*35*). However, their maximum relaxivity per particle was still a factor of 3 lower compared to the Q-SiPaLCs due to a lower payload of the paramagnetic complexes per particle. Similarly, the relaxivity per particle of Q-SiPaLCs is a factor of 40 higher than Mn-doped QDs that were recently reported, despite their high molar relaxivity of 18 mM^{-1} s^{-1} (*47*). Other lipid-based particles, such as liposomes (*48, 49*) or microemulsions (*50*), are capable of carrying a much higher payload of Gd-chelates (typically 25 000 to 100 000 molecules) and therefore exhibit a higher relaxivity per particle. On the other hand, such particles are considerably larger (100 to 250 nm). Apart from r1, we also determined the transverse relaxivity r2. The r2/r1 ratio determines whether a contrast agent is more suitable for T1-weighted or for T2-weighted MRI. This value was determined to be 1.6 for our nanoparticulate contrast agent and therefore can be considered an effective T1 agent.

The characterization of the Q-SiPaLCs shows that they form a very promising particle for dual modality imaging. A crucial aspect for application, however, is their ability to be targeted to specific cell types. To demonstrate the targeting potential of

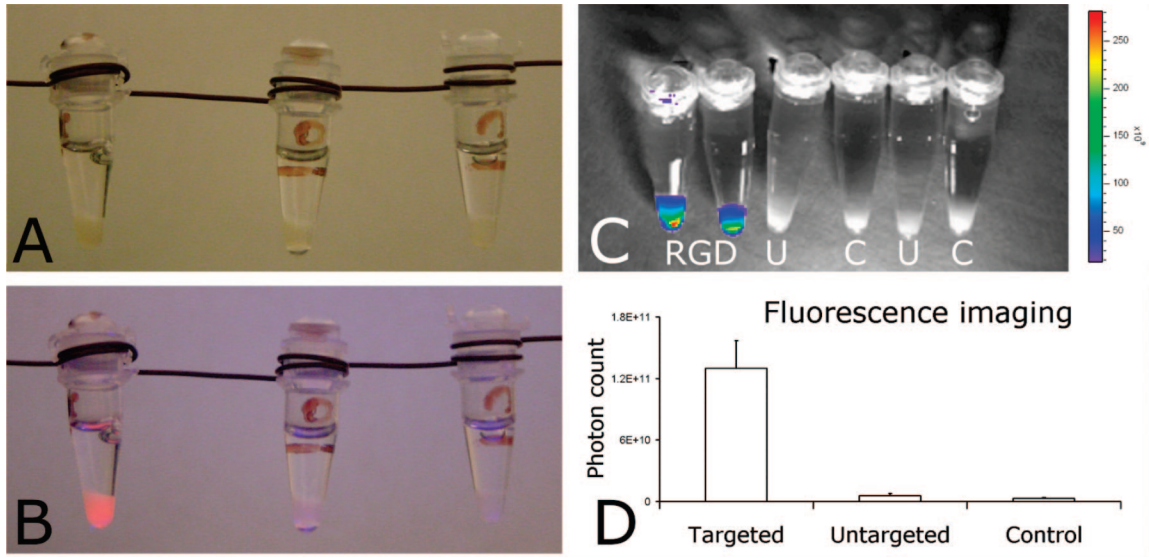

Figure 3. Pellets of cells incubated with RGD-conjugated targeted Q-SiPaLCs (left), non-conjugated untargeted Q-SiPaLCs (middle), and untreated control cells (right) (A) in daylight and (B) illuminated with 365 nm UV. (C) Overlay of a black/white photograph and quantitative fluorescence image of the different cell pellets under UV illumination at 365 nm (RGD = targeted, U = untargeted, C = control cells). The emission intensity from U and C is too low (less than 20×10^9 counts) to be displayed by one of the colors in the scalebar. (D) Mean photon counts of the different cell pellets.

this nanoparticle, it was tested on serum-activated human umbilical vein endothelial cells (HUVEC) in vitro. Nanoparticles can be targeted to these cells by conjugation of multiple RGD-peptides to the maleimide exposing PEG-lipids. These tripeptides specifically bind to $\alpha v\beta 3$-integrin, an adhesion molecule that is expressed by proliferating HUVEC (*51*). This receptor is also predominantly present at angiogenically activated blood vessels, such as those present in tumors (*52*), and has been used for identification of angiogenesis with molecular imaging (*51*). We conjugated ~650 RGD-peptides per particle using a method described previously (*39*). In short, thiol exposing peptides were covalently linked to the distal ends of maleimide-functionalized PEG lipids incorporated in the outer lipid layer of the particle. To assess the specificity of the contrast agent, HUVEC were incubated with either RGD-functionalized nanoparticles (targeted) or non-functionalized nanoparticles (untargeted, no RGD), or they were not incubated with nanoparticles (control). We first established the optimal incubation time on a limited number of cells. Thereafter, incubations were done for 7 h at 37 °C in tissue culture flasks containing $\sim 1.5 \times 10^6$ HUVEC ($n = 2$). Subsequently, cells were washed twice with PBS and fixed with 4% paraformaldehyde solution. In Figure 2A,B, bright-field and fluorescence microscopy images are shown of HUVEC that were incubated with RGD-conjugated nanoparticles. The Q-SiPaLCs are clearly associated with the cells and were found to be internalized at a perinuclear location. Fluorescence images of HUVEC incubated with untargeted Q-SiPaLCs (no functionalization by RGD) showed marginal or no fluorescence (Figure 2C,D), similar to the untreated control cells (not shown). These results demonstrate that lipid-coated QD/silica particles conjugated with RGD peptides are actively taken up by the activated endothelial cells, and that nonspecific uptake (even after 7 h of incubation) is negligible.

Next, the cells were collected and transferred into small Eppendorf cups. In daylight, there is no visual difference between the different loosely packed cell pellets (Figure 3A). Under UV illumination (365 nm), only the cells that had been incubated with RGD conjugated Q-SiPaLCs exhibit a bright red fluorescence and could clearly be distinguished from the two other cell pellets (Figure 3B). In addition, we performed quantitative fluorescence imaging on the different cell pellets (Figure 3C) using the Xenogen IVIS-200. An external illumination source of 365 nm was used, while the photon count was acquired using a spectral imaging filter of 620 nm. In Figure 3D, the mean photon counts of cell pellets incubated with targeted particles, cell pellets incubated with untargeted particles, and control cell pellets are depicted. ~25-fold and ~50-fold differences in photon count were found between the targeted and untargeted cell pellets and the targeted and control pellets, respectively.

Finally, MRI was performed on these cell pellets. A T1-weighted image of the different cell pellets is depicted in Figure 4A and clearly demonstrates higher signal intensity for the pellet of cells incubated with the RGD-conjugated Q-SiPaLCs (the bright white circle) as compared to the control cell pellets (gray circles). In addition, T1 relaxation times were determined in order to allow a more quantitative evaluation of Q-SiPaLCs as a MRI contrast agent. The mean values were 1706 ms, 2189 ms, and 2460 ms, for cells incubated with the targeted particles, cells incubated with untargeted particles, and untreated cells, respectively. The differences in relaxation rate R1 (1/T1) between control cell pellets and cell pellets that were incubated with the nanoparticles correlate with the concentration of contrast agent in the cell pellets. Therefore, we calculated these differences in mean relaxation rates between the control cell pellets and the targeted or untargeted cell pellets. The values clearly demonstrate the effective and specific targeting of this nanoparticulate agent to angiogenically activated endothelial cells (Figure 4B). (Scan parameters are in the Experimental Procedures section.)

DISCUSSION

The Q-SiPaLCs reported here demonstrate the integration of multiple imaging properties in a single bioapplicable nanoparticle and the specific uptake by living cells. This nanoparticulate probe has several advantages over existing agents in terms of detection sensitivity (contrast) due to the high fluorescence quantum yield (35%) and high relaxivity. It presents a new and versatile platform for a wide range of contrast agents suitable for multimodality imaging. Although the QDs were incorporated in silica, more effort needs to be attributed to developing novel stable QD formulations that are not based on Cd to further reduce toxicity. In addition, for in vivo fluorescence imaging

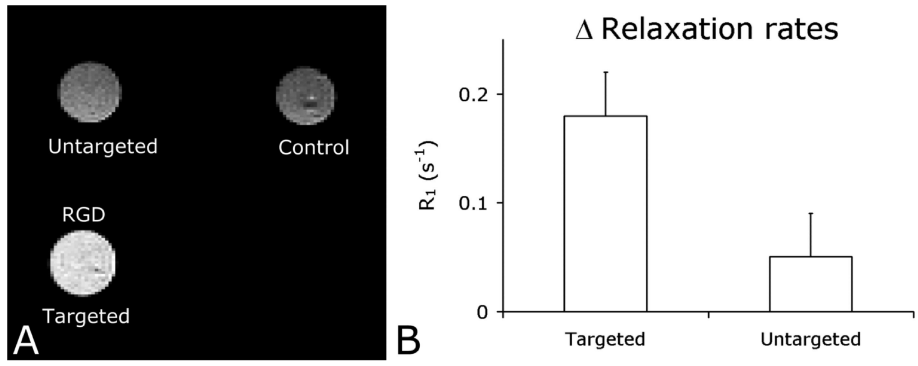

Figure 4. (A) T1-weighted MRI of the different cell pellets (same pellets as displayed in Figure 3) revealed specific uptake of the targeted nanoparticles. (B) Difference in relaxation rates (R1) of the targeted and untargeted cell pellets compared to the relaxation rate of the control cell pellet (set to zero). The differences in relaxation rate reflect the concentration of contrast agent in the untargeted and targeted cell pellets.

purposes, fluorophores that emit photons with a wavelength between 700 and 800 nm have significant advantages, especially for deep tissue imaging (*53*). Therefore, this platform would be more widely applicable if further modified to emit in the near-infrared.

In biomedical research, the two main applications of nanoparticles are their use as carriers for drugs and diagnostic active materials. Their size varies from a few nanometers (QDs, iron oxide nanoparticles, micelles) (*39, 54, 55*) up to hundred nanometers (liposomes) (*2*) and even several hundred nanometers (microemulsions) (*50*) to micrometers (microbubbles) (*56*). Depending on the application and, importantly, the targeted site (vascular versus extravascular), the size may dictate effectiveness. For example, in a study by Stroh et al. it was shown that QD containing silica particles of different sizes (100 nm versus 500 nm) extravasate from the vasculature into the tumor to differing extents (*57*). Furthermore, size also dictates the clearance pathway of nanoparticles and has a significant effect on the circulation half-life. A recent study by Choi et al. (*58*) has revealed renal clearance of particles with a hydrodynamic diameter of less than 5.5 nm. Such small particles are therefore cleared from the circulation relatively fast as compared to, e.g., long-circulating liposomes. The latter platform has a typical size range of 100 to 200 nm and is used extensively in the field of drug targeting, both preclinically and clinically (*2*). The advantage of the current platform in terms of particle size is twofold. First, the nanoparticles are highly monodisperse, as a result of the reverse micelle method used to grow a silica shell of a well-defined thickness. Another great advantage of our particles is that they can be easily and accurately tuned to any desired size from ~20 nm to over 1 μm, by increasing the diameter of the silica spheres. The silica shell is also expected to prevent leaking of Cd and thus reduce the cytotoxicity due to the Cd-containing quantum dots. In addition, any desired fluorescence color or a combination of colors can be chosen to allow for multiplexing or "bar-coding" (*59*), by inserting different kinds of QDs in the silica spheres. Furthermore, due to the high surface area of the Q-SiPaLCs, a high payload of Gd-DTPA-DSA lipids can be integrated per particle. Therefore, the relaxivity per particle is high and can even be increased significantly by increasing the size of the silica particle. Target specificity can be introduced using PEG-lipids with a functional moiety, like maleimide used in this study. The number of functional groups can be varied, which allows the creation of a particle with multiple ligands. This can increase the targeting efficiency of the particle due to multivalent interactions. This is an important issue, since it was recently reported that the target specificity of maleimide-targeted QDs may be poor when a single QD contains less that 1 target peptide per QD, making the uptake highly nonspecific, especially due to the small size of a single QD (*60*). The design of our Q-SiPaLCs solves this problem, because of the possibility of attaching multiple ligands per particle. Furthermore, the nonspecific uptake of the Q-SiPaLCs by HUVEC is shown to be negligible in this study. The nanoparticles as designed in the present report can be applied for imaging of ongoing angiogenesis as a diagnostic tool in the management of cancer. Next to the RGD-peptides used in this study, other ligands, such as antibodies (*61*), antibody fragments (*62*), or proteins (*63*) may be conjugated in a similar fashion. The PEG-lipids that surround the Q-SiPaLCs ensure good pharmacokinetics and an improved biocompatibility of the nanoparticles.

Finally, the presently reported contrast agent design offers numerous possibilities to integrate a wide range of properties for multimodality imaging. We have successfully demonstrated a general and effective pathway for making silica (nano)spheres bioapplicable and target-specific. We have recently investigated the biocompatibility and biodistribution properties of the Q-SiPaLCs. In vitro, an elevated cell vitality was shown for the lipid-coated particles as compared to the bare particles, while in vivo the lipid-coated QD/silica particles displayed increased circulation half-lives as a result of a diminished reticuloendothelial system clearance rate (*64*). In the future, this method can be applied to any combination of contrast agents incorporated in silica to make them suitable for biomedical applications. For example, magnetite nanoparticles (for MRI detection), gold or bismuth nanoparticles (for CT or EM detection), or fluorescent materials (QDs, dyes, phosphor nanocrystals) can readily be integrated in silica and can be made bioapplicable through the procedure reported here. Additional properties may be added to the particle by inserting paramagnetic or fluorescent amphiphiles in the lipidic coating, for example. Drug delivery and gene targeting may also be functionalities that can be accomplished using this biocompatible silica nanoparticle platform.

In summary, we have developed a new method for making bioapplicable silica nanoparticles that can serve as a contrast agent for target-specific multimodality imaging. The nanoparticle is composed of a QD incorporated in a silica sphere of 31 nm. First, the silica surface is made hydrophobic, and subsequently, it is surrounded by pegylated, paramagnetic, and biofunctional lipids. This results in a highly monodisperse, fluorescent, and paramagnetic contrast agent suitable for both fluorescence imaging and MRI studies, and it shows a highly specific uptake by HUVEC. The use of the presently reported method for creating biocompatible and target-specific silica nanoparticles opens a new platform for multimodality imaging contrast agents by integrating any desired combination of contrast agents in the silica nanoparticle and inserting (combinations of) functional amphiphiles in the lipidic coating.

ACKNOWLEDGMENT

Partial support was provided by NIH/NHLBI R01 HL71021, NIH/ NHLBI R01 HL78667 (Z.A.F.), and the Peter Jay Sharp Foundation (W.J.M.M.)

LITERATURE CITED

(1) Sinha, R., Kim, G. J., Nie, S., and Shin, D. M. (2006) Nanotechnology in cancer therapeutics: bioconjugated nanoparticles for drug delivery. *Mol. Cancer. Ther. 5*, 1909–17.

(2) Torchilin, V. P. (2005) Recent advances with liposomes as pharmaceutical carriers. *Nat. Rev. Drug Discovery 4*, 145–60.

(3) Moghimi, S. M., Hunter, A. C., and Murray, J. C. (2005) Nanomedicine: current status and future prospects. *Faseb J. 19*, 311–30.

(4) Bulte, J. W., and Kraitchman, D. L. (2004) Iron oxide MR contrast agents for molecular and cellular imaging. *NMR Biomed. 17*, 484–99.

(5) Sitharaman, B., Kissell, K. R., Hartman, K. B., Tran, L. A., Baikalov, A., Rusakova, I., Sun, Y., Khant, H. A., Ludtke, S. J., Chiu, W., Laus, S., Toth, E., Helm, L., Merbach, A. E., and Wilson, L. J. (2005) Superparamagnetic gadonanotubes are high-performance MRI contrast agents. *Chem. Commun.* 3915–17.

(6) Kim, D., Park, S., Lee, J. H., Jeong, Y. Y., and Jon, S. (2007) Antibiofouling polymer-coated gold nanoparticles as a contrast agent for in vivo x-ray computed tomography imaging. *J. Am. Chem. Soc. 129*, 7661–65.

(7) Michalet, X., Pinaud, F. F., Bentolila, L. A., Tsay, J. M., Doose, S., Li, J. J., Sundaresan, G., Wu, A. M., Gambhir, S. S., and Weiss, S. (2005) Quantum dots for live cells, in vivo imaging, and diagnostics. *Science 307*, 538–44.

(8) Wickline, S. A., Neubauer, A. M., Winter, P. M., Caruthers, S. D., and Lanza, G. M. (2007) Molecular imaging and therapy of atherosclerosis with targeted nanoparticles. *J. Magn. Reson. Imaging 25*, 667–80.

(9) Mulder, W. J. M., Griffioen, A. W., Strijkers, G. J., Cormode, D. P., Nicolay, K., and Fayad, Z. A. (2007) Magnetic and fluorescent nanoparticles for multimodality imaging. *Nanomedicine 2*, 307–24.

(10) Darbandi, M., Thomann, R., and Nann, T. (2005) Single quantum dots in silica spheres by microemulsion synthesis. *Chem. Mater. 17*, 5720–25.

(11) Selvan, S. T., Tan, T. T., and Ying, J. Y. (2005) Robust, non-cytotoxic, silica-coated CdSe quantum dots with efficient photoluminescence. *Adv. Mater. 17*, 1620–25.

(12) Graf, C., Vossen, D. L. J., Imhof, A., and van Blaaderen, A. (2003) A general method to coat colloidal particles with silica. *Langmuir 19*, 6693–700.

(13) Liz-Marzan, L. M., Giersig, M., and Mulvaney, P. (1996) Synthesis of nanosized gold-silica core-shell particles. *Langmuir 12*, 4329–35.

(14) Philipse, A. P., Vanbruggen, M. P. B., and Pathmamanoharan, C. (1994) Magnetic silica dispersions - preparation and stability of surface-modified silica particles with a magnetic core. *Langmuir 10*, 92–99.

(15) Sathe, T. R., Agrawal, A., and Nie, S. M. (2006) Mesoporous silica beads embedded with semiconductor quantum dots and iron oxide nanocrystals: Dual-function microcarriers for optical encoding and magnetic separation. *Anal. Chem. 78*, 5627–32.

(16) Kim, J., Lee, J. E., Lee, J., Yu, J. H., Kim, B. C., An, K., Hwang, Y., Shin, C. H., Park, J. G., and Hyeon, T. (2006) Magnetic fluorescent delivery vehicle using uniform mesoporous silica spheres embedded with monodisperse magnetic and semiconductor nanocrystals. *J. Am. Chem. Soc. 128*, 688–89.

(17) Yi, D. K., Selvan, S. T., Lee, S. S., Papaefthymiou, G. C., Kundaliya, D., and Ying, J. Y. (2005) Silica-coated nanocomposites of magnetic nanoparticles and quantum dots. *J. Am. Chem. Soc. 127*, 4990–91.

(18) Salgueiriño-Maceira, V., Correa-Duarte, M. A., Spasova, M., Liz-Marzán, L. M., and Farle, M. (2006) Composite silica spheres with magnetic and luminescent functionalities. *Adv. Funct. Mater. 16*, 509–14.

(19) van Blaaderen, A., and Vrij, A. (1992) Synthesis and characterization of colloidal dispersions of fluorescent, monodisperse silica spheres. *Langmuir 8*, 2921–31.

(20) Burns, A., Ow, H., and Wiesner, U. (2006) Fluorescent core-shell silica nanoparticles: towards "Lab on a Particle" architectures for nanobiotechnology. *Chem. Soc. Rev. 35*, 1028–42.

(21) Ow, H., Larson, D. R., Srivastava, M., Baird, B. A., Webb, W. W., and Wiesner, U. (2005) Bright and stable core-shell fluorescent silica nanoparticles. *Nano Lett. 5*, 113–17.

(22) Lu, C. W., Hung, Y., Hsiao, J. K., Yao, M., Chung, T. H., Lin, Y. S., Wu, S. H., Hsu, S. C., Liu, H. M., Mou, C. Y., Yang, C. S., Huang, D. M., and Chen, Y. C. (2007) Bifunctional magnetic silica nanoparticles for highly efficient human stem cell labeling. *Nano Lett. 7*, 149–54.

(23) Rieter, W. J., Kim, J. S., Taylor, K. M. L., An, H. Y., Lin, W. L., Tarrant, T., and Lin, W. B. (2007) Hybrid silica nanoparticles for multimodal Imaging. *Angew. Chem., Int. Ed. 46*, 3680–82.

(24) Yoon, T. J., Yu, K. N., Kim, E., Kim, J. S., Kim, B. G., Yun, S. H., Sohn, B. H., Cho, M. H., Lee, J. K., and Park, S. B. (2006) Specific targeting, cell sorting, and bio-imaging with smart magnetic silica core-shell nanomaterials. *Small 2*, 209–15.

(25) Wang, L., Wang, K. M., Santra, S., Zhao, X. J., Hilliard, L. R., Smith, J. E., Wu, J. R., and Tan, W. H. (2006) Watching silica nanoparticles glow in the biological world. *Anal. Chem. 78*, 646–54.

(26) Lu, J., Liong, M., Zink, J. I., and Tamanoi, F. (2007) Mesoporous silica nanoparticles as a delivery system for hydrophobic anticancer drugs. *Small 3*, 1341–46.

(27) Insin, N., Tracy, J. B., Lee, H., Zimmer, J. P., Westervelt, R. M., and Bawendi, M. G. (2008) Incorporation of iron oxide nanoplarticles and quantum dots into silica microspheres. *ACS Nano 2*, 197–202.

(28) Bridot, J. L., Faure, A. C., Laurent, S., Riviere, C., Billotey, C., Hiba, B., Janier, M., Josserand, V., Coll, J. L., VanderElst, L., Muller, R., Roux, S., Perriat, P., and Tillement, O. (2007) Hybrid gadolinium oxide nanoparticles: multimodal contrast agents for in vivo imaging. *J. Am. Chem. Soc. 129*, 5076–84.

(29) Taylor, K. M. L., Kim, J. S., Rieter, W. J., An, H., Lin, W. L., and Lin, W. B. (2008) Mesoporous silica nanospheres as highly efficient MRI contrast agents. *J. Am. Chem. Soc. 130*, 2154–55.

(30) Chen, F. Q., and Gerion, D. (2004) Fluorescent CdSe/ZnS nanocrystal-peptide conjugates for long-term, nontoxic imaging and nuclear targeting in living cells. *Nano Lett. 4*, 1827–32.

(31) Gerion, D., Pinaud, F., Williams, S. C., Parak, W. J., Zanchet, D., Weiss, S., and Alivisatos, A. P. (2001) Synthesis and properties of biocompatible water-soluble silica-coated CdSe/ZnS semiconductor quantum dots. *J. Phys. Chem. B 105*, 8861–71.

(32) Jana, N. R., Earhart, C., and Ying, J. Y. (2007) Synthesis of water-soluble and functionalized nanoparticles by silica coating. *Chem. Mater. 19*, 5074–82.

(33) Selvan, S. T., Patra, P. K., Ang, C. Y., and Ying, J. Y. (2007) Synthesis of silica-coated semiconductor and magnetic quantum dots and their use in the imaging of live cells. *Angew. Chem., Int. Ed. 46*, 2448–52.

(34) Wolcott, A., Gerion, D., Visconte, M., Sun, J., Schwartzberg, A., Chen, S. W., and Zhang, J. Z. (2006) Silica-coated CdTe quantum dots functionalized with thiols for bioconjugation to IgG proteins. *J. Phys. Chem. B 110*, 5779–89.

(35) Gerion, D., Herberg, J., Bok, R., Gjersing, E., Ramon, E., Maxwell, R., Kurhanewicz, J., Budinger, T. F., Gray, J. W., Shuman, M. A., and Chen, F. F. (2007) Paramagnetic silica-coated nanocrystals as an advanced MRI contrast agent. *J. Phys. Chem. C 111*, 12542–51.

(36) de Mello Donega, C., Bode, M., and Meijerink, A. (2006) Size- and temperature-dependence of exciton lifetimes in CdSe quantum dots. *Phys. Rev. B 74*, 085320.

(37) Xie, R. G., Kolb, U., Li, J. X., Basche, T., and Mews, A. (2005) Synthesis and characterization of highly luminescent CdSe-Core CdS/Zn0.5Cd0.5S/ZnS multishell nanocrystals. *J. Am. Chem. Soc. 127*, 7480–88.

(38) van Helden, A. K., Jansen, J. W., and Vrij, A. (1981) Preparation and characterization of spherical monodisperse silica dispersions in nonaqueous solvents. *J. Colloid Interface Sci. 81*, 354–68.

(39) Mulder, W. J. M., Koole, R., Brandwijk, R. J., Storm, G., Chin, P. T. K., Strijkers, G. J., de Mello Donega, C., Nicolay, K., and Griffioen, A. W. (2006) Quantum dots with a paramagnetic coating as a bimodal molecular imaging probe. *Nano Lett. 6*, 1–6.

(40) Koole, R., van Schooneveld, M. M., Hilhorst, J., Donega, C. D., 't Hart, D. C., van Blaaderen, A., Vanmaekelbergh, D., and Meijerink, A. (2008) On the incorporation mechanism of hydrophobic quantum dots in silica spheres by a reverse microemulsion method. *Chem. Mater. 20*, 2503–12.

(41) Awasthi, V. D., Garcia, D., Klipper, R., Goins, B. A., and Phillips, W. T. (2004) Neutral and anionic liposome-encapsulated hemoglobin: Effect of postinserted poly(ethylene glycol)-distearoylphosphatidylethanolamine on distribution and circulation kinetics. *J. Pharmacol. Exp. Ther. 309*, 241–48.

(42) Litzinger, D. C., Brown, J. M., Wala, I., Kaufman, S. A., Van, G. Y., Farrell, C. L., and Collins, D. (1996) Fate of cationic liposomes and their complex with oligonucleotide in vivo. *Bba-Biomembranes 1281*, 139–49.

(43) Dubertret, B., Skourides, P., Norris, D. J., Noireaux, V., Brivanlou, A. H., and Libchaber, A. (2002) In vivo imaging of quantum dots encapsulated in phospholipid micelles. *Science 298*, 1759–62.

(44) Aime, S., Botta, M., Fasano, M., and Terreno, E. (1998) Lanthanide(III) chelates for NMR biomedical applications. *Chem. Soc. Rev. 27*, 19–29.

(45) Petrache, H. I., Dodd, S. W., and Brown, M. F. (2000) Area per lipid and acyl length distributions in fluid phosphatidylcholines determined by 2H NMR spectroscopy. *Biophys. J. 79*, 3172–92.

(46) Prinzen, L., Miserus, R. J. J. H. M., Dirksen, A., Hackeng, T. M., Deckers, N., Bitsch, N. J., Megens, R. T. A., Douma, K., Heemskerk, J. W., Kooi, M. E., Frederik, P. M., Slaaf, D. W., van Zandvoort, M. A. M. J., and Reutelingsperger, C. P. M. (2007) Optical and magnetic resonance imaging of cell death and platelet activation using annexin A5-functionalized quantum dots. *Nano Lett. 7*, 93–100.

(47) Wang, S., Jarrett, B. R., Kauzlarich, S. M., and Louie, A. Y. (2007) Core/shell quantum dots with high relaxivity and photoluminescence for multimodality imaging. *J. Am. Chem. Soc. 129*, 3848–56.

(48) Mulder, W. J. M., Strijkers, G. J., Griffioen, A. W., van Bloois, L., Molema, G., Storm, G., Koning, G. A., and Nicolay, K. (2004) A liposomal system for contrast-enhanced magnetic resonance imaging of molecular targets. *Bioconjugate Chem. 15*, 799–806.

(49) Mulder, W. J. M., Strijkers, G. J., van Tilborg, G. A. F., Griffioen, A. W., and Nicolay, K. (2006) Lipid-based nanoparticles for contrast-enhanced MRI and molecular imaging. *NMR Biomed. 19*, 142–64.

(50) Lanza, G. M., Winter, P. M., Caruthers, S. D., Hughes, M. S., Cyrus, T., Marsh, J. N., Neubauer, A. M., Partlow, K. C., and Wickline, S. A. (2006) Nanomedicine opportunities for cardiovascular disease with perfluorocarbon nanoparticles. *Nanomedicine 1*, 321–29.

(51) Mulder, W. J., Strijkers, G. J., Habets, J. W., Bleeker, E. J., van der Schaft, D. W., Storm, G., Koning, G. A., Griffioen, A. W., and Nicolay, K. (2005) MR molecular imaging and fluorescence microscopy for identification of activated tumor endothelium using a bimodal lipidic nanoparticle. *Faseb J. 19*, 2008–10.

(52) Brooks, P. C., Clark, R. A. F., and Cheresh, D. A. (1994) Requirement of vascular integrin alpha(V)beta(3) for angiogenesis. *Science 264*, 569–71.

(53) Ntziachristos, V., Ripoll, J., Wang, L. V., and Weissleder, R. (2005) Looking and listening to light: the evolution of whole-body photonic imaging. *Nat. Biotechnol. 23*, 313–20.

(54) van Tilborg, G. A. F., Mulder, W. J. M., Deckers, N., Storm, G., Reutelingsperger, C. P. M., Strijkers, G. J., and Nicolay, K. (2006) Annexin A5-functionalized bimodal lipid-based contrast agents for the detection of apoptosis. *Bioconjugate Chem. 17*, 741–49.

(55) Mulder, W. J. M., Strijkers, G. J., Briley-Saboe, K. C., Frias, J. C., Aguinaldo, J. G. S., Vucic, E., Amirbekian, V., Tang, C., Chin, P. T. K., Nicolay, K., and Fayad, Z. A. (2007) Molecular imaging of macrophages in antherosclerotic plaques using bimodal PEG-micelles. *Magn. Reson. Med. 58*, 1164–70.

(56) Kaufmann, B. A., Sanders, J. M., Davis, C., Xie, A., Aldred, P., Sarembock, I. J., and Lindner, J. R. (2007) Molecular imaging of inflammation in atherosclerosis with targeted ultrasound detection of vascular cell adhesion molecule-1. *Circulation 116*, 276–84.

(57) Stroh, M., Zimmer, J. P., Duda, D. G., Levchenko, T. S., Cohen, K. S., Brown, E. B., Scadden, D. T., Torchilin, V. P., Bawendi, M. G., Fukumura, D., and Jain, R. K. (2005) Quantum dots spectrally distinguish multiple species within the tumor milieu in vivo. *Nat. Med. 11*, 678–82.

(58) Choi, H. S., Liu, W., Misra, P., Tanaka, E., Zimmer, J. P., Ipe, B. I., Bawendi, M. G., and Frangioni, J. V. (2007) Renal clearance of quantum dots. *Nat. Biotechnol. 25*, 1165–70.

(59) Xu, H. X., Sha, M. Y., Wong, E. Y., Uphoff, J., Xu, Y. H., Treadway, J. A., Truong, A., O'Brien, E., Asquith, S., Stubbins, M., Spurr, N. K., Lai, E. H., and Mahoney, W. (2003) Multiplexed SNP genotyping using the Qbead (TM) system: a quantum dot-encoded microsphere-based assay. *Nucleic Acids Res. 31*, 1–10, e43.

(60) Pathak, S., Davidson, M. C., and Silva, G. A. (2007) Characterization of the functional binding properties of antibody conjugated quantum dots. *Nano Lett. 7*, 1839–45.

(61) Mulder, W. J., Strijkers, G. J., Griffioen, A. W., van Bloois, L., Molema, G., Storm, G., Koning, G. A., and Nicolay, K. (2004) A liposomal system for contrast-enhanced magnetic resonance imaging of molecular targets. *Bioconjugate Chem. 15*, 799–806.

(62) Kang, H. W., Josephson, L., Petrovsky, A., Weissleder, R., and Bogdanov, A., Jr. (2002) Magnetic resonance imaging of inducible E-selectin expression in human endothelial cell culture. *Bioconjugate Chem. 13*, 122–7.

(63) van Tilborg, G. A., Mulder, W. J., Chin, P. T., Storm, G., Reutelingsperger, C. P., Nicolay, K., and Strijkers, G. J. (2006) Annexin A5-conjugated quantum dots with a paramagnetic lipidic coating for the multimodal detection of apoptotic cells. *Bioconjugate Chem. 17*, 865–8.

(64) van Schooneveld, M. M., Vucic, E., Koole, R., Zhou, Y., Stocks, J., Cormode, D. P., Tang, C. Y., Gordon, R. E., Nicolay, K., Meijerink, A., Fayad, Z. A., and Mulder, W. J. M. (2008) Improved biocompatibility and pharmacokinetics of silica nanoparticles by means of a lipid coating: a multimodality investigation. *Nano Lett. 8*, 2517–25.

BC800368X